Vibration welding of ABS to itself and to polycarbonate, poly(butylene terephthalate), poly(ether imide) and modified poly(phenylene oxide)

V. K. Stokes* and S. Y. Hobbs
GE Corporate Research and Development, Schenectady, NY 12301, USA
(Received 5 February 1992; revised 13 August 1992)

In contrast to some thermoplastics, in which weld strengths equal to those of the base resins can be achieved, tests on two grades of acrylonitrile–butadiene–styrene resin (ABS) show weld strengths on the order of 90–95% of the strength of ABS, with slightly higher values being obtained at lower rubber levels. Welds of ABS to four other thermoplastics are shown to have strengths in the range of 65–83% of the strength of ABS, the weakest of the five thermoplastics. The welding of ABS to bisphenol-A polycarbonate is examined in detail. Optical, scanning and transmission electron microscopy are used to characterize the morphology of the weld.

(Keywords: welding; vibration welding; weld strength; thermoplastics; ABS; polycarbonate; poly(butylene terephthalate); poly(etherimide); modified poly(phenylene oxide))

INTRODUCTION

In vibration welding of thermoplastics, frictional work done by vibrating two parts under pressure, along their common interface, is used to generate heat to effect welds[1]. Typical vibration welds of neat thermoplastic resins exhibit the four phases[1,2] schematically shown in *Figure 1*. In phase I, Coulomb friction generates heat at the interface, raising its temperature to the point at which the polymer can undergo viscous flow. In phase II, the interface begins to melt and the mechanism of heat generation changes from solid Coulomb friction to dissipation in the molten polymer. The molten polymer begins to flow in a lateral direction, resulting in an increase in the weld penetration — the distance by which the parts approach each other as a result of lateral flow. In phase III, the melting and flow are at a steady state, and the weld penetration increases linearly with time. When the machine is shut off, the weld penetration continues to increase because the weld pressure causes the molten film to flow until it solidifies; this is phase IV. Past work on welding has focused on characterizing the effects of weld parameters, such as the weld frequency, the weld amplitude, the weld pressure and the weld time, on the welding process and the strength of welds for several different thermoplastics, including bisphenol-A polycarbonate (PC), poly(butylene terephthalate) (PBT), poly(ether imide) (PEI) and modified poly(phenylene oxide) (M-PPO)[1–4]. That work has shown that the most important parameter affecting the *static* weld strength is the weld penetration. Very high static weld strengths, equal to that of the base resin, can be achieved when the penetration exceeds a critical threshold, and the weld strength drops off for penetrations below this value. This threshold is affected by the thickness of the part being welded; the threshold increases with part thickness[5]. The weldability of the dissimilar amorphous polymers PC and PEI and the weldability of PC to the semicrystalline PBT have been studied[6,7]. The effects of chopped-glass fillers on the weld process and weld strength have been evaluated[8], and the welding of structural foams has been addressed[9]. Additional penetration into the steady-state phase does not affect weld strength in neat resins[3,4]; this is also true of structural foams[9]. However, the strengths of welds between dissimilar materials can continue to increase[6,7].

Weld pressure can have opposite effects on the weld strengths of resins. For example, while the strengths of

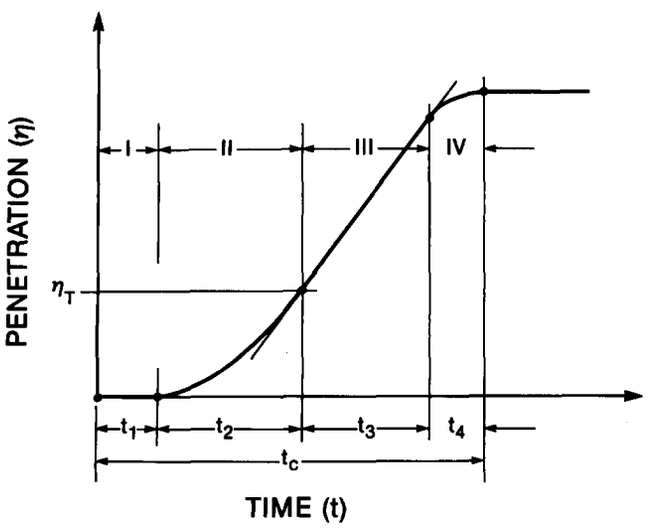

Figure 1 Schematic penetration–time curve showing the four phases of vibration welding

*To whom correspondence should be addressed

0032-3861/93/061222-10

PEI welds increase with weld pressure, the strengths of M-PPO welds decrease rapidly with increasing weld pressure[4]. Of the four resins — PC, PBT, PEI and M-PPO — PEI is the only one which requires high-frequency (250–400 Hz) welding for the welds to attain neat resin level strength[4].

In PC, PBT, PEI and M-PPO, weld strengths equal to that of the neat resin can be achieved easily[3,4], and this is also true of structural foams[9]. Also, in welds of PC/PEI and those of PC/PBT, weld strength equal to that of the weaker of the two materials can be achieved[6,7]. In glass-filled materials, however, the weld strength is lower than that of the glass-filled material[8]. A study of the vibration welding of two commercially available grades of impact modified PC/PBT blends have shown that, while both grades can achieve room-temperature weld strengths equal to that of the blends, resin-level low-temperature weld strength can only be achieved in the blend with the higher impact-modifier content[10].

The literature on the welding of dissimilar materials is quite small and is mainly concerned with hot-tool welding[11,12]. The hot-tool butt welding of dissimilar high-density polyethylene (HDPE) has been discussed[13,14]. Some information is also available on the relationship between the structure and mechanical properties of polypropylene (PP) homopolymer to PP copolymer bonds[15]. However, except for vibration welding[6,7], information is not available on the weldability of dissimilar materials for any of the other welding methods.

While static strength (obtained by a tensile test in which the displacement or strain or load increases at a uniform rate until failure) is an important indicator of weld quality, it is not the only measure. In some applications creep rupture may be more important, for which the time to rupture at different stress levels may be the appropriate measure of weld quality[16]. Process conditions can have a large effect on the morphology of the weld zone, which in turn can affect impact performance[17]. As such, in some applications impact strength may be a more important measure of weld quality than static weld strength. Some data on the fatigue strength of vibration-welded butt joints of PC, PBT, PEI and M-PPO are available[18].

This paper is concerned with the vibration welding of acrylonitrile–butadiene–styrene resin (ABS) to itself and several other thermoplastics: bisphenol-A polycarbonate (PC), an amorphous polymer; poly(butylene terephthalate) (PBT), a semicrystalline polymer; poly(ether imide) (PEI), a high temperature amorphous polymer; a poly(phenylene oxide)/high-impact polystyrene blend (M-PPO); and glass-filled M-PPO (GF-MPPO). The weld strengths of the various resin pairs are evaluated in terms of various welding parameters including frequency, pressure and penetration. In the case of ABS/ABS and ABS/PC welds, the weld morphologies and their relationship to weld performance are examined in some detail.

EXPERIMENTAL

Materials

The materials used were commercially available resins. ABS was supplied in the form of CYCOLAC* GPM 5600 (~20% rubber), which will be referred to as ABS, and CYCOLAC GPP 4600 (~14% rubber), which will be referred to as ABS-X. PC was obtained as LEXAN* 9030, PBT* as VALOX 325, PEI as ULTEM* 1000, M-PPO as NORYL* 190, and GF-MPPO as NORYL GFN2.

Welding

All of the test data in this paper were obtained from specimens cut from PC extruded sheet material (5.8 mm in thickness), and injection moulded plaques of the six other polymers: ABS, ABS-X and GF-MPPO (6.1 mm in thickness); PBT and PEI (6.35 mm in thickness); and M-PPO (5.08 mm in thickness). The edges of each specimen were machined to obtain rectangular blocks of size 76.2 mm × 25.4 mm × thickness for assuring accurate alignment of the surfaces during butt welding.

All of the welds were made on a research vibration welding machine[1]. Weld tests were terminated at varying preset values of the weld penetration. Because the weld pressure causes the molten film to flow until it solidifies, the final penetration η_F at the end of the weld is larger than the preset value η_0. Throughout this paper, penetration data refer to this final penetration η_F. The bulk of the welds in this paper were done at a frequency n of 120 Hz and a weld amplitude of $a = 1.59$ mm. Some welds on ABS were also made at $n = 250$ Hz and $a = 0.44$ mm.

Details of the weld procedure have been described previously[3]. Two specimens with machined lateral edges were vibration welded along the 25.4 mm × thickness edges, resulting in a bar 152.4 mm × 25.4 mm × thickness, which was then routed down to a standard ASTM D638 tensile test specimen with the vibration-welded butt joint in its centre (Figure 2 in Ref. 3).

The tensile bar, which had a uniform transverse butt weld at mid-length, was then subjected to a constant-displacement-rate tensile test in which the strain across the weld was monitored with an extensometer. This made it possible to monitor the average failure strain over the 25.4 mm gauge length of the extensometer, across the weld. All of the weld strength tensile tests in this paper were done at a nominal strain rate of 0.01 s^{-1}.

As in earlier work[3–10], the weld flash or 'bead' was not removed. Also, the weld strengths reported in this paper were obtained by dividing the load at failure by the original cross-sectional area of the specimen. Because of large local deformations, the true failure stress would, in most cases, be larger than the nominal stress data in this paper.

Furthermore, the 25.4 mm gauge-length extensometer can grossly underestimate the local strain in the failure region once strain localization sets in, therefore the significance of the reported failure strains ε_0 should be interpreted with care. These values only represent the lower limit of the failure strain at the weld.

The slight mismatches in the thicknesses of the specimens of ABS and the other thermoplastics — the largest difference of 1.02 mm being between ABS and M-PPO — could affect the strength of the joints. But the consequent stress concentration caused by this mismatch would make the strength data in this paper conservative. Strengths of mixed welds are based on the cross-sectional area of the thinner of the two specimens welded.

Microscopy

The ABS/ABS welds produced were analysed by

* CYCOLAC, LEXAN, VALOX, ULTEM and NORYL are registered trademarks of the General Electric Company

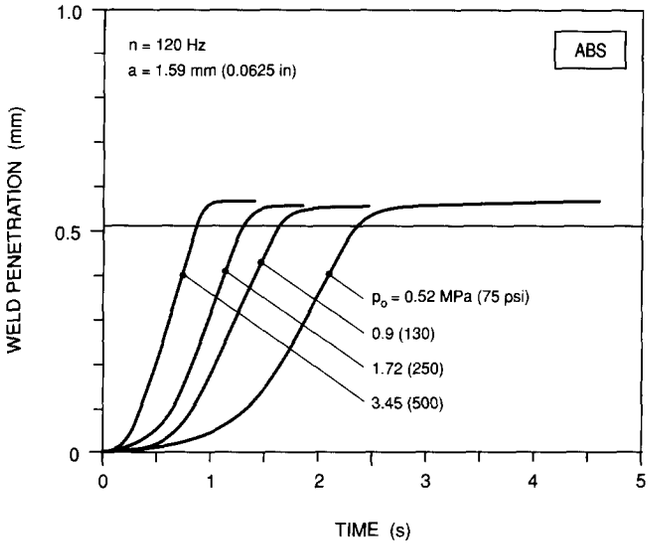

Figure 2 Penetration–time curves for ABS welds for $n=120$ Hz and $a=1.59$ mm with the weld pressure as parameter

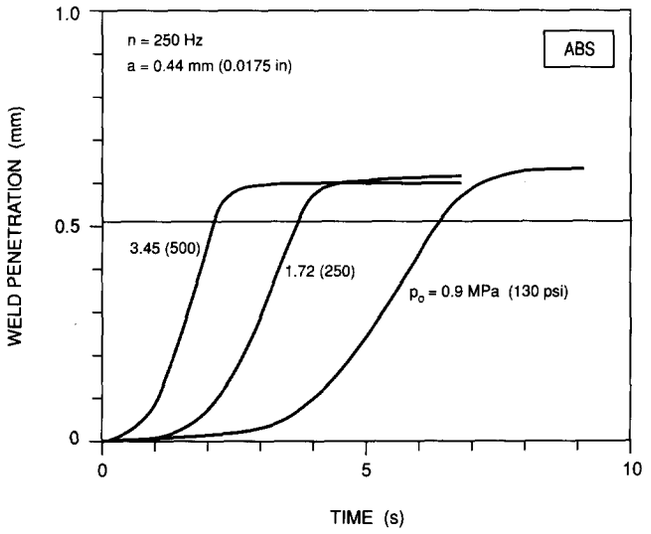

Figure 3 Penetration–time curves for ABS welds for $n=250$ Hz and $a=0.44$ mm with the weld pressure as parameter

transmission electron microscopy (TEM) and the ABS/PC welds by a combination of TEM, optical microscopy (OM) and scanning electron microscopy (SEM). Both intact and broken specimens were examined. A number of sample preparation and observation procedures were used to highlight specific structural features. For TEM studies, cross sections were cut from the intact welded specimens using a small saw. In the case of the broken specimens, a thin layer of epoxy was applied to the fracture surface prior to cutting, to minimize deformation adjacent to the fracture plane. The welds were stained by overnight immersion in a 2% aqueous solution of OsO_4 to highlight the dispersed rubber phase. After staining, the samples were microtomed at room temperature using a Reichart Ultracut E ultramicrotome equipped with a diamond knife. In the case of the ABS/PC welds, the sections were additionally exposed to RuO_4 vapour to differentiate the PC and styrene–acrylonitrile (SAN) phases. All observations were carried out on a Hitachi H-600 TEM.

The ABS/PC welds were also examined by SEM and OM. Cross sections were prepared by metallographic polishing. These were examined directly by OM and, after etching in an O_2 plasma or treatment with OsO_4, by SEM. In the latter case an annular backscatter detector was employed to highlight chemical contrast differences between the various phases. Fracture surfaces were examined directly by SEM after sputtering with Au/Pd. SEM observations were carried out in a Jeol 840 SEM and OM observations on a Zeiss stereo microscope.

RESULTS

ABS/ABS welds

Penetration–time data. Representative penetration–time curves for $n=120$ Hz, $a=1.59$ mm welds of ABS — at three weld pressures of $p_0=0.52$, 0.9 and 3.45 MPa — are shown in *Figure 2*. Corresponding penetration–time curves for $n=250$ Hz, $a=0.44$ mm welds are shown in *Figure 3*. Clearly, the curves in these two figures exhibit the four phases of vibration welding which have been observed in several neat and filled resins. Steady-state penetration data for these and additional tests on ABS are listed in *Table 1*.

Weld strength. Strength and ductility data for $n=120$ Hz, $a=1.59$ mm welds of ABS for weld pressures of $p_0=0.26$, 0.52, 0.9, 1.72 and 3.45 MPa are listed in *Table 2* for cutoff penetrations of $\eta_0=0.13$, 0.25 and

Table 1 Steady-state penetration rates for ABS/ABS welds

Frequency, n (Hz)	Amplitude, a (mm)	Weld pressure, p_0 (MPa)	Penetration rate, $\dot{\eta}$ (mm s^{-1})
120	1.59	0.52	0.45
120	1.59	0.9	0.56
120	1.59	1.72	0.68
120	1.59	3.45	0.84
250	0.44	0.9	0.21
250	0.44	1.72	0.30
250	0.44	3.45	0.40

Table 2 Strength and ductility of welds of ABS 6.1 mm thick at a strain rate of $\dot{\varepsilon}=0.1\,s^{-1}$ ($n=120$ Hz; $a=1.59$ mm)

p_0 (MPa)	η_F (mm)	t_0 (s)	σ_w (MPa)	σ_w/σ_{ABS} (%)	ε_0 (%)
0.26	0.61	4.81	36.0	81.7	1.76
0.26	0.61	4.81	35.7	80.9	1.78
0.34	0.60	3.53	34.3	77.9	–
0.34	0.60	3.53	34.3	77.9	–
0.52	0.22	1.54	37.6	85.3	1.93
0.52	0.19	1.37	36.7	83.4	1.89
0.52	0.33	1.99	39.7	90.2	2.09
0.52	0.33	2.24	39.8	90.3	2.22
0.52	0.33	1.94	38.6	87.7	2.19
0.52	0.61	2.74	39.7	90.1	2.15
0.52	0.58	2.43	39.7	90.2	2.04
0.9	0.19	1.33	37.7	85.6	1.96
0.9	0.33	1.28	37.3	84.6	1.96
0.9	0.34	1.66	37.1	84.3	1.88
0.9	0.58	1.81	36.9	83.9	1.80
1.72	0.18	0.79	36.3	82.4	1.78
1.72	0.32	1.02	37.1	84.1	1.79
1.72	0.57	1.41	37.5	85.1	1.86
3.45	0.19	0.53	35.1	79.7	1.72
3.45	0.33	0.68	36.9	83.9	1.72
3.45	0.58	0.98	37.2	84.4	1.80

p_0, weld pressure; η_F, final penetration; t_0, time of vibration; σ_w, weld strength; σ_w/σ_{ABS}, relative strength based on ultimate strength of $\sigma_{ABS}=44$ MPa for ABS; ε_0, nominal failure strain

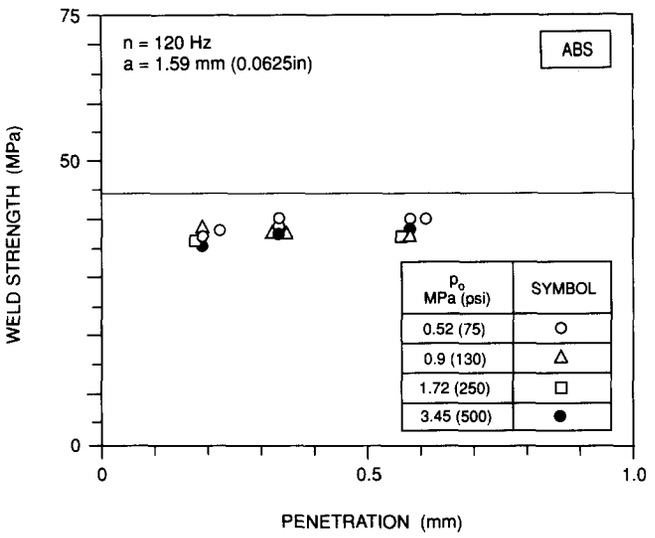

Figure 4 Strength of 120 Hz welds of ABS *versus* the penetration for a weld amplitude of 1.59 mm, with the weld pressure as parameter

Table 3 Strength and ductility of welds of ABS 6.1 mm thick at a strain rate of $\dot{\varepsilon}=0.01\,s^{-1}$ ($n=250$ Hz; $a=0.44$ mm)

p_0 (MPa)	η_F (mm)	t_0 (s)	σ_w (MPa)	σ_w/σ_{ABS} (%)	ε_0 (%)
0.9	0.22	4.35	36.8	83.5	1.76
0.9	0.37	4.86	35.9	81.5	1.65
0.9	0.65	6.66	37.6	85.3	1.82
1.72	0.20	2.82	35.7	81.1	1.65
1.72	0.36	3.46	34.3	77.9	1.54
1.72	0.61	3.92	35.7	81.0	1.65
3.45	0.19	1.45	32.2	73.1	1.51
3.45	0.33	1.97	31.5	71.5	1.46
3.45	0.60	2.31	30.4	68.9	1.42

Nomenclature as in *Table 2*

0.51 mm. For the wide range of conditions studied, the highest strength achieved was 90.3% of the strength of ABS. The nominal failure strain corresponding to this test, $\varepsilon_0=2.22\%$, also had the highest value. The variations of the weld strength *versus* the penetration are shown in *Figure 4*, in which the thin horizontal line corresponds to the strength of ABS (44.1 MPa). The highest strengths were achieved at a weld pressure of 0.52 MPa.

In order to improve the weld strength, welds were also done at 250 Hz at $a=0.44$ mm. The corresponding data are listed in *Table 3*. The highest strength achieved was about 85% of the strength of ABS, which is not an improvement over the strength of 120 Hz welds.

In order to assess the effect of the rubber content on weld performance, a limited number of tests at $n=120$ Hz, $a=1.27$ mm and $p_0=0.9$ MPa were done at $\eta_0=0.13$, 0.25 and 0.51 mm. The corresponding strength and ductility data are listed in *Table 4*. A higher relative strength of 94.5% was obtained for ABS-X, which has a lower rubber content (~14%), compared to 87.8% for ABS, which has a higher rubber content (~20%).

Morphology. Cross sections cut from the ABS/ABS welds and observed by TEM revealed a modest degree of rubber orientation in the vibration direction parallel to the weld plane. This characteristic is visible on comparing the photomicrographs in *Figure 5a* and *b*. Most of the rubber particles in the weld zone were somewhat elongated with the ratio between the maximum and minimum diameters (d_{max}/d_{min}) lying somewhere between 1.5/1 and 1.8/1. Some more heavily stained rubber particles, believed to be less heavily crosslinked, were more severely elongated and are indicated by arrows in *Figure 5b*. By implication, a similar degree of orientation is expected in the SAN matrix resin close to the weld plane. There was no evidence of incomplete melting, large-scale voiding or other macroscopic defects in any of the welds examined.

Cross sections cut from broken ABS/ABS welds showed extensive crazing and cavitation of the rubber particles in the regions adjacent to the fracture surfaces. These features are shown in *Figure 6*. By themselves, crazing and void formation are unremarkable, being typically observed in deformed ABS specimens containing no welds. It is significant, however, that among the various welded resins that have been studied, ABS is the only one which fails primarily by crazing rather than shear flow. Both the craze initiation and propagation stresses are known to be lowered when there is molecular alignment parallel to the craze plane. The combination of these factors is believed to account for the somewhat diminished strength of the ABS/ABS welds compared with those measured for more ductile matrix resins.

Welds of ABS to PC, PBT, PEI and M-PPO

This section discusses the process phenomenology and weld strengths associated with the welding of ABS to PC, PBT, PEI and M-PPO. The welding of ABS to PC is studied in more detail than the welding of ABS to the other resins.

Process phenomenology. Representative penetration–time curves for $n=120$ Hz, $a=1.59$ mm welds of ABS to PC, PBT, PEI and M-PPO are shown in *Figure 7*, for $p_0=0.9$ and 3.45 MPa. The tests were run to higher penetrations of $\eta_0=1.27$ mm because the strength of welds of dissimilar materials can continue to increase even after an apparent steady state has been attained[6]. All these curves exhibit the four phases of vibration welding. Steady-state penetration data for three tests are listed in *Table 5*.

Given the scatter that can be expected in experimental data, the penetration–time curves for ABS/PC, ABS/PBT and ABS/PEI for $p_0=0.9$ MPa are almost the same, as are the corresponding steady-state penetration rates

Table 4 Strength and ductility of two grades of ABS (effect of rubber content) at a strain rate of $\dot{\varepsilon}=0.01\,s^{-1}$ ($n=120$ Hz; $a=1.27$ mm; $p_0=0.9$ MPa)

Approximate rubber content (%)	η_F (mm)	t_0 (s)	σ_w (MPa)	σ_w/σ_u (%)	ε_0 (%)
20	0.19	1.12	37.0	84.0[a]	1.96
20	0.33	1.58	38.7	87.8[a]	2.15
20	0.57	1.83	38.3	87.1[a]	2.06
14	0.18	2.28	43.1	94.5[b]	1.83
14	0.33	2.33	43.1	94.6[b]	2.17
14	0.61	2.96	38.9	85.4[b]	2.11

Nomenclature as in *Table 2*
[a] Based on an ultimate strength of $\sigma_u=44.1$ MPa
[b] Based on an ultimate strength of $\sigma_u=45.5$ MPa

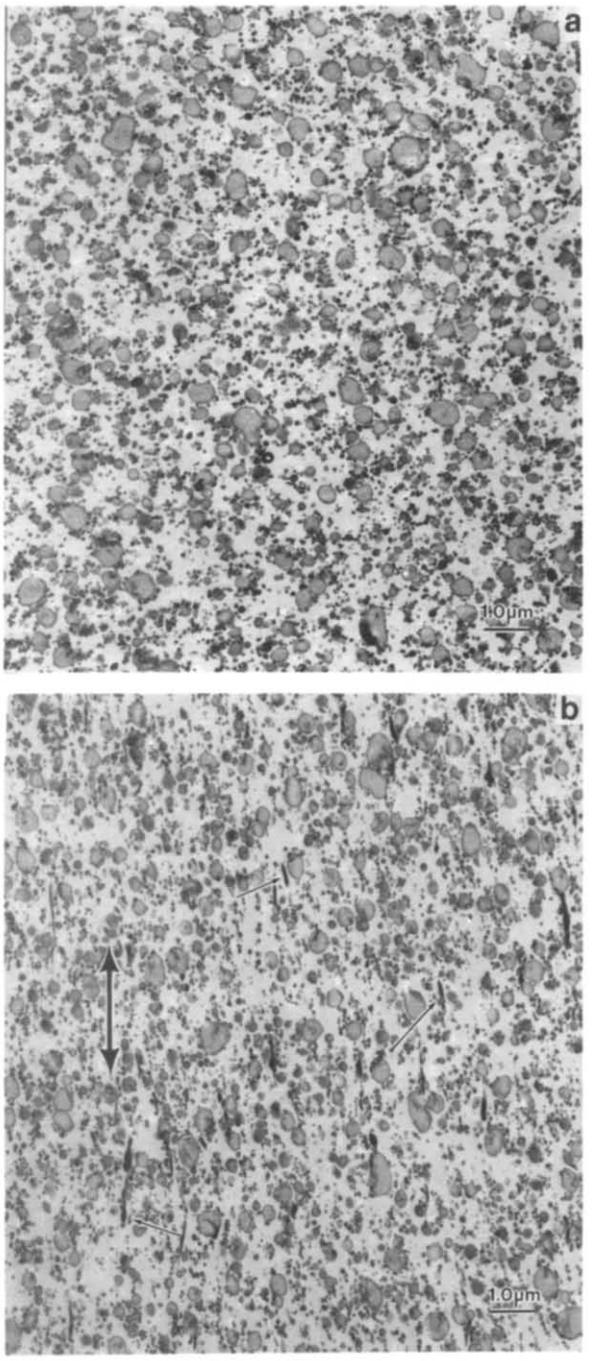

Figure 5 (a) TEM photograph, OsO_4 stained cross section cut from core of ABS bar away from the weld zone. Note absence of rubber orientation. (b) TEM photograph, OsO_4 stained cross section cut from ABS/ABS weld ($n=120$ Hz; $a=1.59$ mm; $p_0=0.9$ MPa). Vibration direction indicated by large arrow and highly elongated rubber particles by smaller arrows

(*Table 5*). This is also true for $p_0=3.45$ MPa, for which the difference between the curves for ABS/PC and ABS/PBT is insignificant. In view of the differences between the physical properties of these polymers, these results imply that the bulk of the melting in these mixed-material welds is occurring in the ABS specimen. The higher penetration rate for ABS/M-PPO is consistent with the lower softening temperature of M-PPO relative to PBT (~150°C compared to 235°C) and the lower melt viscosity of MPO relative to PC and PEI.

Strength of ABS/PC welds. Strength and ductility data for 120 Hz welds of ABS/PC for $a=1.59$ mm, at $p_0=0.9$ and 3.45 MPa, are listed in *Table 6*. The relative strengths in the fifth column have been obtained by dividing the weld strength by the strength of ABS ($\sigma_{ABS}=44.1$ MPa), the weaker of the two materials. The

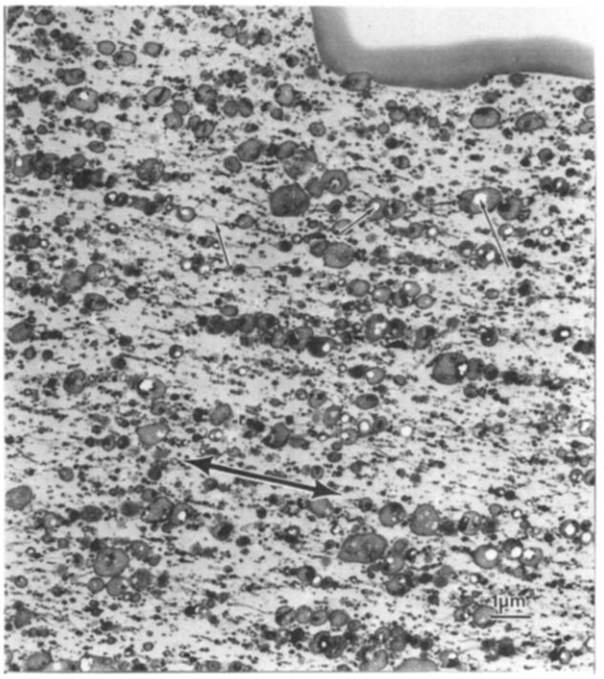

Figure 6 TEM photograph, OsO_4 stained cross section cut from fractured ABS/ABS weld ($n=120$ Hz; $a=1.59$ mm; $p_0=0.9$ MPa). Large arrow indicates vibration direction; smaller arrows mark crazes and cavitated rubber particles

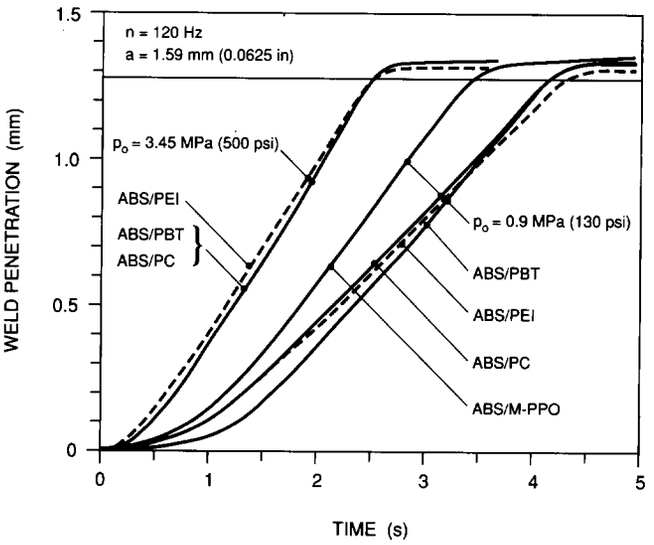

Figure 7 Penetration–time curves for ABS/PC, ABS/PBT, ABS/PEI and ABS/M-PPO welds for $n=120$ Hz and $a=1.59$ mm, at two weld pressures

Table 5 Comparison of steady-state penetration rates of welds of ABS to itself and to PC, PBT, PEI and M-PPO ($n=120$ Hz; $a=1.59$ mm)

p_0 (MPa)	Penetration rate, $\dot{\eta}$ (mm s^{-1})				
	ABS/ABS	ABS/PC	ABS/PBT	ABS/PEI	ABS/M-PPO
0.9	0.56	0.40	0.44	0.37	0.5
3.45	0.84	0.62	0.65	0.58	–

Table 6 Strength and ductility of ABS/PC welds at a strain rate of $\dot{\varepsilon}=0.01\,s^{-1}$ ($n=120$ Hz; $a=1.59$ mm)

p_0 (MPa)	η_F (mm)	t_0 (s)	σ_w (MPa)	σ_w/σ_{ABS} (%)	σ_w/σ^*_{ABS} (%)	ε_0 (%)
0.9	0.30	1.61	31.5	71.5	79.2	1.40
0.9	0.71	2.65	32.0	72.6	80.4	1.40
0.9	1.37	4.28	36.4	82.6	91.5	1.72
3.45	0.30	1.02	32.8	74.6	82.6	1.48
3.45	0.72	1.58	32.8	74.5	82.5	1.48
3.45	1.33	2.57	31.8	72.3	80.1	1.40

Nomenclature as in *Table 2*
σ^*_{ABS} = 39.8 MPa is the highest strength attained in ABS/ABS welds

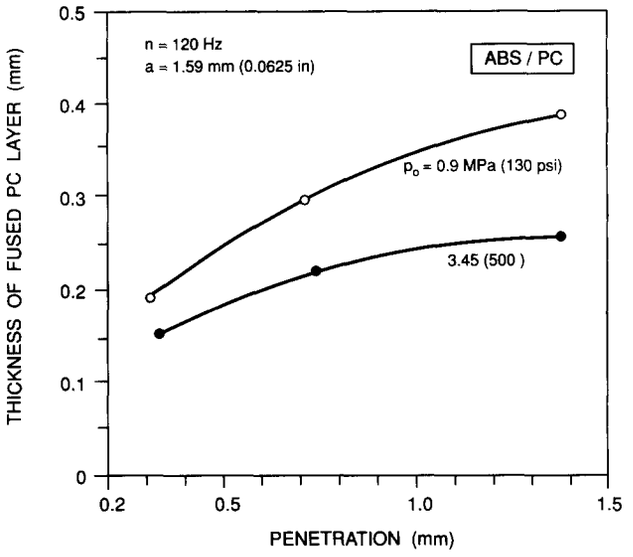

Figure 8 Variation in thickness of fused PC layer with weld pressure and penetration

highest strength attained in ABS/ABS welds (*Table 2*) is $\sigma^*_{ABS}=39.8$ MPa, which corresponds to a relative strength of $\sigma_w/\sigma_{ABS}=90.3\%$. A more representative relative strength for ABS/PC welds is therefore σ_w/σ^*_{ABS}, which is listed in the sixth column in *Table 6*.

At the lower pressure (0.9 MPa), the strength increases with the penetration, even after an apparent steady state has been attained at a penetration of about $\eta=0.3$ mm, just as in PC/PEI welds[6]. The strengths at penetrations of 0.3 and 0.71 mm are about the same, whereas that at $\eta_F=1.37$ mm is significantly higher, thereby indicating that the PC has begun to undergo sufficient melting and flow. The penetration does not appear to affect weld strength at the higher pressure of 3.45 MPa up to a penetration of 1.33 mm. Clearly, it is possible to achieve weld strengths in ABS/PC on the order of about 90% of the strength of ABS/ABS welds.

Morphology of ABS/PC welds. Initial examinations of the flashed regions in the ABS/PC welds showed that almost all of the lateral flow of resin had taken place in the ABS phase. Even at the highest penetrations and pressures, the PC halves of the weld exhibited only small lips of resin at the periphery of the weld plane while the ABS halves showed large build-ups of flash. As in other welds carried out using PC, the thickness of the resin layer heated above the glass transition temperature, T_g, could be ascertained from the position of the refractive index discontinuity in the PC phase. These values are plotted as a function of penetration for the two sets of welding conditions in *Figure 8*.

In both the 0.9 MPa and 3.45 MPa welds, the thickness of the PC 'melt' zone increased with penetration and welding time although it remained consistently thinner at the higher pressure. A photomicrograph showing the relative sizes of the flashed regions of PC and ABS as well as the refractive index discontinuity in the PC phase is shown in *Figure 9*.

Closer inspection of the welds by SEM showed that the turbulent mixing patterns, previously observed in the PC/PEI and PC/PBT welds[6,7], were absent. Regardless of the welding conditions, the PC/ABS weld planes were relatively featureless and devoid of the convoluted structures which had developed in the earlier studies at higher amplitudes and pressures. A typical example is shown in *Figure 10*. The low level of mechanical mixing at the weld plane is ascribed to the marked differences in the viscosity–shear rate behaviour of the two resins. Whereas PC is relatively Newtonian, ABS shows significant shear thinning at higher deformation rates. To illustrate this point, the viscosity–shear rate curves for the two resins used in this study, measured at 220°C and 240°C, are superimposed in *Figure 11*. During vibration welding, the maximum shear rate, estimated from the known vibration amplitude and frequency and the melt zone thickness, is on the order of several hundred s^{-1}. In this range the viscosity of PC is six to eight times that of ABS. Thus the highest levels of deformation and lateral flow of resin will occur in the ABS side of the weld. As a result, mechanical mixing is minimized and large amounts of ABS flash develop.

It is interesting to note that the relative amounts of PC and ABS flash correlate most strongly with the high frequency response characteristics of the two resins. This observation implies that squeeze flow, induced by external pressure applied to the two halves of the

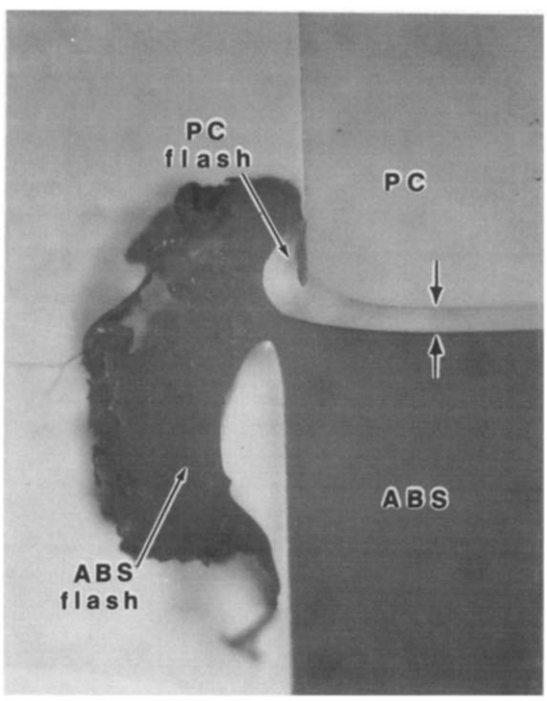

Figure 9 Optical micrograph, oblique illumination, showing relative sizes of PC and ABS flash and PC refractive index discontinuity in sample welded at 3.45 MPa with 0.71 mm penetration

specimen during welding, is not the mechanism by which melted resin is removed from the melt zone. Instead, it appears that a thin film of resin (principally ABS) shear thins during each oscillation and is immediately displaced to the weld periphery as the sample moves back and forth. Flash thus builds up in a series of tiny waves rather than being continuously exuded. Such waves are, in fact, visible on inspecting the flashed areas in the electron microscope (*Figure 12*).

The resin/rubber ratio in the ABS adjacent to the ABS/PC weld plane was characterized from back-scattered SEM images of stained cross sections such as that shown in *Figure 13*. In this photomicrograph, the rubber phase appears bright as the result of chemical contrast differences produced by reaction of the rubber with OsO_4. By digitizing and binarizing images of this type, the relative area fractions of rubber and SAN lying in bands parallel to the weld plane could be determined. These computations were performed using a PGT IMIX imaging processing system on bands having a thickness

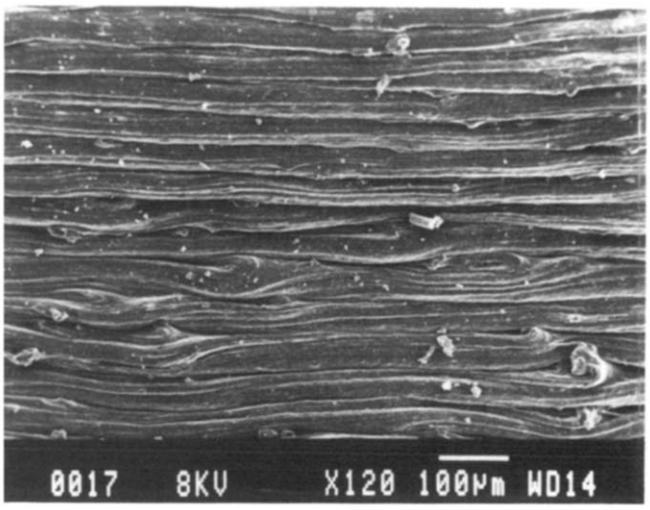

Figure 12 SEM photograph showing rippled surface on ABS flash produced by vibration waves

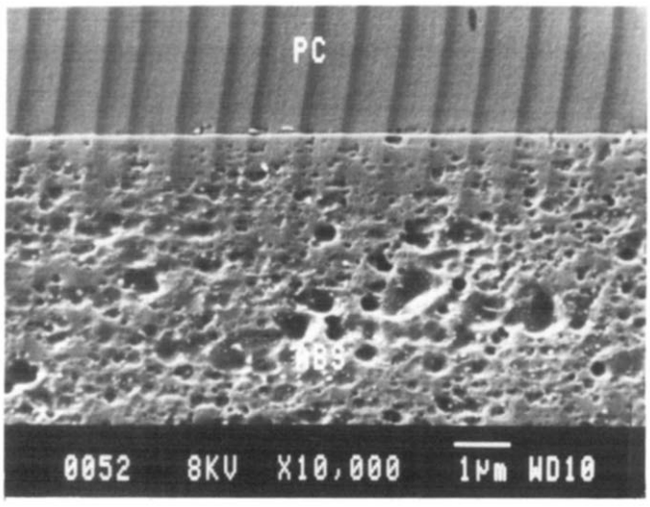

Figure 10 SEM photograph, plasma-etched cross section, showing absence of interfacial mixing in sample welded at 0.9 MPa with 1.37 mm penetration. The interfacial cross sections of samples welded under all other conditions were similar

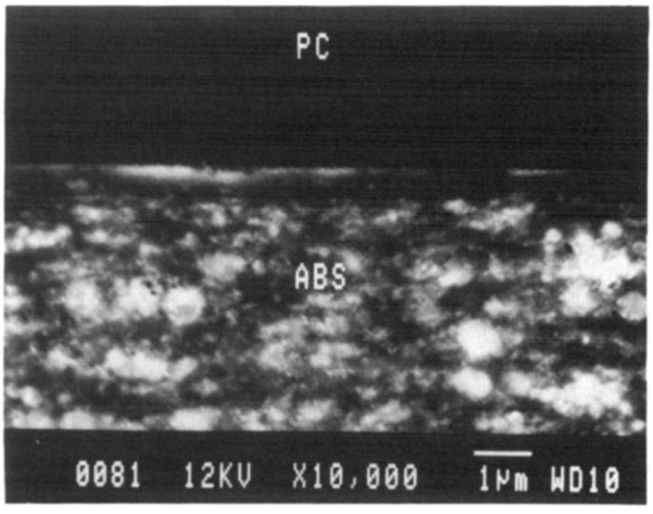

Figure 13 SEM photograph, backscattered electron image of osmium-stained cross section, showing the distribution of rubber particles (light areas) in the ABS phases of a weld produced at 3.45 MPa with 0.30 mm penetration. Some stretched-out rubber domains can be seen at the interface (arrow)

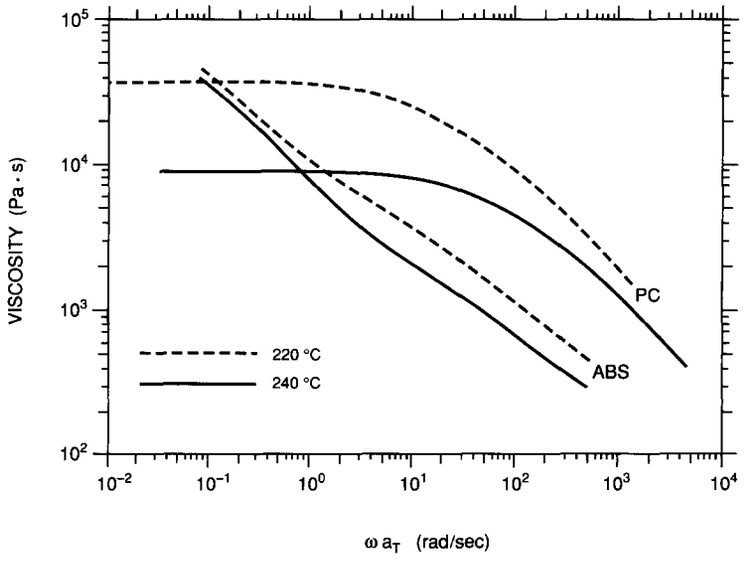

Figure 11 Viscosity–shear rate curves for PC and ABS at 220°C and 240°C

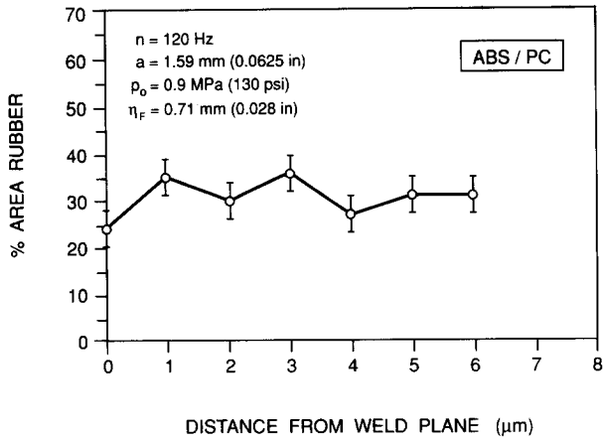

Figure 14 Plot showing the resin/rubber ratio in ABS layers lying parallel to the weld plane

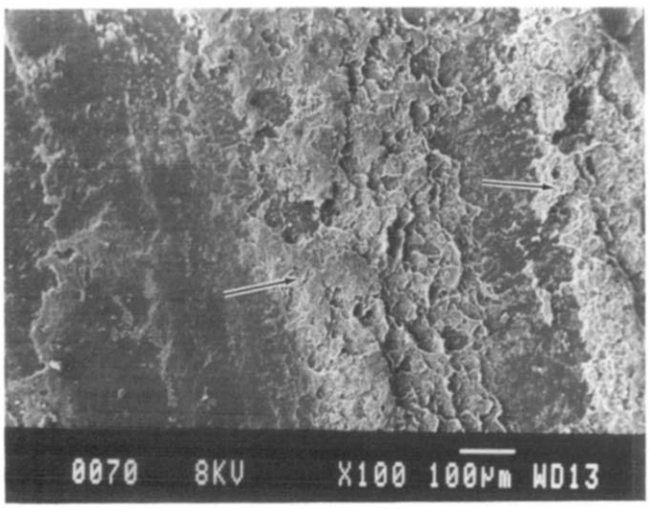

Figure 15 SEM photograph, PC half of weld fracture surface, showing islands of ABS (arrows) remaining attached to the PC substrate

of 1.0 μm and length of 30 μm and averaged over eight viewing fields. The results, shown in *Figure 14* for a weld carried out at 0.9 MPa and having a penetration of 0.71 mm, are typical of those obtained and show there is no significant enrichment of rubber or resin near the weld interface.

It is worth noting that, for all the curves, the maximum area fraction of rubber exceeds that expected from the resin composition although the area and volume fractions are normally expected to be equivalent[19]. This discrepancy is produced by some backscattered electrons that are emitted from rubber domains lying just below the surface. These add to signals arising from domains on the surface and produce an apparent elevation in the rubber level. Since this process occurs uniformly over the viewing surface, it does not affect foregoing conclusions, although the true rubber fractions will typically be displaced downwards from those shown in *Figure 14*.

In tensile tests, all of the welded specimens broke at or very close to the weld plane. A typical SEM photograph, taken of the PC half of a 3.45 MPa weld with a penetration of 0.3 mm, is shown in *Figure 15*. The patchy, light areas are composed of ABS and are extensively cavitated as shown in *Figure 16*. This structure contrasts strongly with the smooth appearance of the intervening PC (*Figure 17*). The phase assignments were confirmed by X-ray photoelectron spectroscopy (XPS). Significantly, no PC was observed on any of the ABS halves of the broken specimens by either XPS or SEM.

TEM cross sections, cut from the PC halves of the fractured specimens, showed that the ABS patches remaining on the surface were heavily crazed and that many of the rubber particles were cavitated. These observations are consistent with the voided appearance of the ABS domains seen in the SEM photographs. In a number of instances, rubber particles were visible at the PC/SAN boundary and long crazes could be seen running along the interface (*Figure 18*). In cases where these crazes diverted from the interface they consistently re-entered the ABS phase. This process is believed to produce the patchy ABS structures found on the PC sides of the fracture surface and to account for the absence of PC on the corresponding ABS sides.

Strength of ABS/PBT welds. Strength data for 120 Hz ABS/PBT welds are listed in *Table 7*. As with ABS/PBT

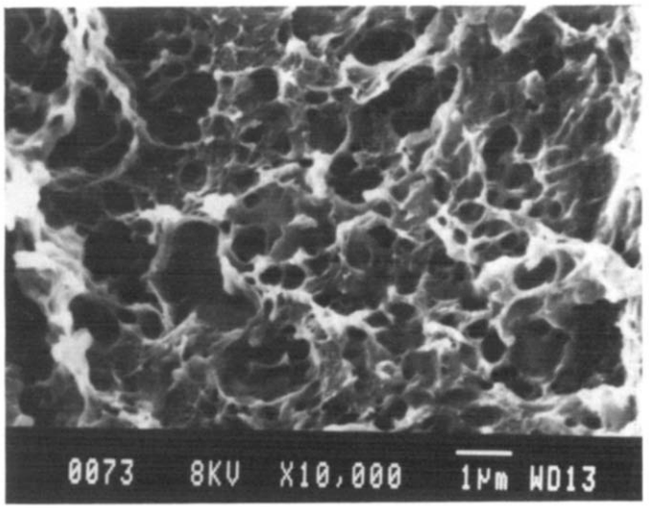

Figure 16 Enlarged area of *Figure 15* showing heavily cavitated structure of ABS islands remaining on PC surface

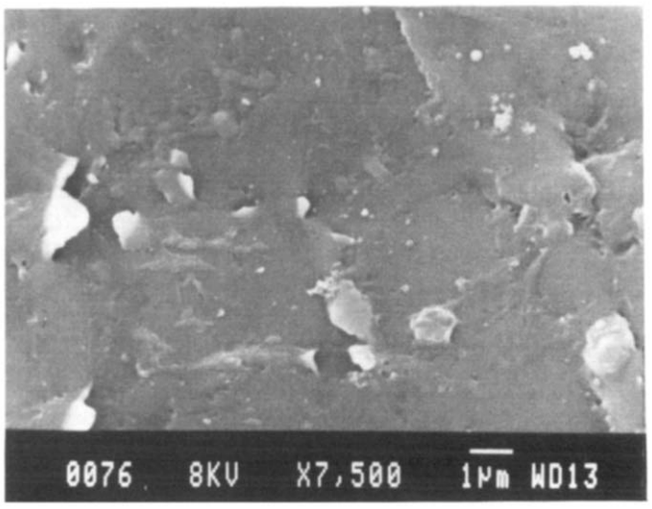

Figure 17 Enlarged area of *Figure 15* showing very smooth PC surface produced by interfacial crack growth

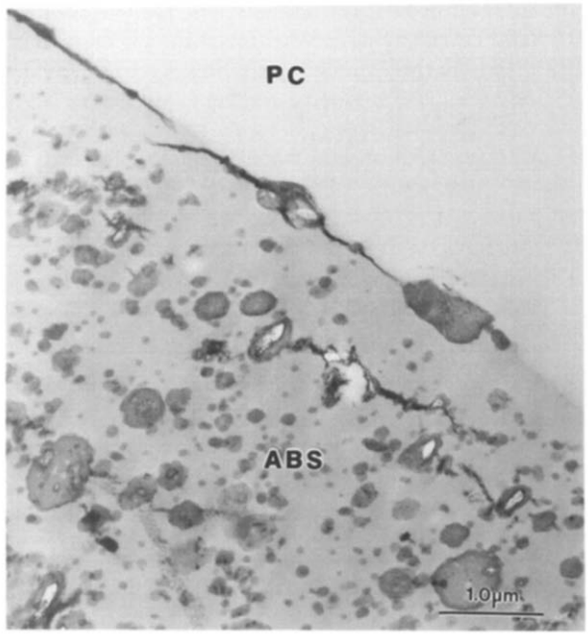

Figure 18 TEM photograph, osmium-stained thin section, showing craze emanating from interfacial rubber particle in broken ABS/PC weld. Other crazes can be see in the ABS phase

Table 7 Strength and ductility of ABS/PBT welds at a strain rate of $\dot{\varepsilon}=0.01\,s^{-1}$ ($n=120$ Hz; $a=1.59$ mm)

p_0 (MPa)	η_F (mm)	t_0 (s)	σ_w (MPa)	σ_w/σ_{ABS} (%)	σ_w/σ^*_{ABS} (%)	ε_0 (%)
0.9	0.32	1.85	24.1	54.7	60.6	0.97
0.9	0.71	2.73	34.1	77.5	85.8	1.44
0.9	1.36	4.32	35.3	80.1	88.7	1.59
3.45	0.32	1.04	8.2	18.7	20.7	0.80
3.45	0.70	1.55	33.4	75.7	83.8	1.37
3.45	1.35	2.58	31.1	70.6	78.2	1.27

Nomenclature as in *Table 2*
σ^*_{ABS} = 39.8 MPa is the highest strength attained in ABS/ABS welds

welds, the weld strength increases steadily with the penetration, even though an apparent steady state is attained at a penetration of about 0.45 mm. Here again, a higher strength is achieved at the lower pressure of 0.9 MPa. Weld strengths of ABS/PBT welds on the order of 89% of ABS/ABS welds can be achieved.

Strength of ABS/PEI welds. Strength data for 120 Hz welds are listed in *Table 8*. An apparent steady state is attained at a penetration of about 0.3 mm. Surprisingly, the highest strengths are achieved at low penetration levels. Here again, higher strengths are achieved at lower weld pressures, although the effect is not large. Weld strengths of ABS/PEI welds on the order of 72% of the strength of ABS/ABS welds can be achieved.

Strength of ABS/M-PPO and ABS/GF-MPPO welds. A limited set of data for 120 Hz welds of ABS/M-PPO and ABS/GF-MPPO at $a=1.59$ mm and $p_0=0.9$ MPa are listed in *Table 9*. An apparent steady state is achieved at a penetration of about 0.45 mm. The strengths of both ABS/M-PPO and ABS/GF-MPPO welds continue to increase with penetration. Welds of ABS/M-PPO can attain about 85% of the strength of ABS/ABS welds. But the strengths of ABS/GF-MPPO welds are substantially lower, at about 70% of the strength of ABS/ABS welds.

DISCUSSION AND CONCLUSIONS

Of the resins studied thus far (PC, PBT, PEI, M-PPO and PC-PBT), ABS is the only one for which base-resin-level weld strengths have not been achieved. This deficiency is believed to be related to ABS failing primarily by cavitation and crazing rather than by plastic flow. Whereas the molecules in more ductile resins are able to realign under an applied load, this process is restricted in SAN. Because of this restriction, voiding and craze growth tend to become concentrated in the zones of oriented resin and impact modifier adjacent to the weld plane. Eventually a flaw of critical size is produced in this region and the sample fails prematurely.

In PC/ABS welds this process appears to be further enhanced by the presence of rubber particles in the PC/ABS boundary. *Figure 18* provides convincing evidence that cracks can be readily initiated at such particles and propagated along the weld plane. It is reasonable to suspect that growth will tend to be confined to the interface because of the modulus mismatch between the two resins. Such cracks are much less susceptible to interruption by normal processes, such as blunting or bifurcation, than those in bulk ABS. Furthermore, multiple crazes running along the same plane can readily combine to produce a flaw leading to failure. There is no evidence to suggest that there is a depletion of rubber particles in the ABS lying adjacent to the weld plane or that this reduces weld strength. Moreover, the presence of numerous islands of ABS on the PC halves of the fractured specimens indicates that bond strength between the two resins is inherently good. This characteristic is consistent with the known miscibility of PC and SAN resins[20].

For comparison, it is useful to normalize the strengths of mixed-material welds by the strength of ABS, which has the lowest strength of the materials studied. When this is done, the highest per cent relative weld strengths

Table 8 Strength and ductility of ABS/PEI welds at a strain rate of $\dot{\varepsilon}=0.01\,s^{-1}$ ($n=120$ Hz; $a=1.59$ mm)

p_0 (MPa)	η_F (mm)	t_0 (s)	σ_w (MPa)	σ_w/σ_{ABS} (%)	σ_w/σ^*_{ABS} (%)	ε_0 (%)
0.9	0.29	1.68	27.6	62.6	69.3	1.06
0.9	0.67	2.57	28.6	65.0	72.0	1.14
0.9	1.32	4.51	26.1	59.3	65.7	1.02
3.45	0.29	0.88	28.4	64.4	71.3	1.07
3.45	0.69	1.63	25.5	57.9	64.1	1.02
3.45	1.32	2.63	20.2	45.9	50.8	0.75

Nomenclature as in *Table 2*
σ^*_{ABS} = 39.8 MPa is the highest strength attained in ABS/ABS welds

Table 9 Strength and ductility of ABS/M-PPO and ABS/GF-MPPO welds at a strain rate of $\dot{\varepsilon}=0.01\,s^{-1}$ ($n=120$ Hz; $a=1.59$ mm; $p_0=0.9$ MPa)

Weld	η_F (mm)	t_0 (s)	σ_w (MPa)	σ_w/σ_{ABS} (%)	σ_w/σ^*_{ABS} (%)	ε_0 (%)
ABS/M-PPO	0.33	1.53	31.1	70.7	78.3	1.31
ABS/M-PPO	0.60	2.03	33.0	74.8	82.8	1.37
ABS/GF-MPPO	0.29	1.69	22.7	51.4	56.9	0.69
ABS/GF-MPPO	0.56	2.41	23.9	54.4	60.2	0.67
ABS/GF-MPPO	1.33	4.50	27.9	63.4	70.2	0.87

Nomenclature as in *Table 2*
σ^*_{ABS} = 39.8 MPa is the highest strength attained in ABS/ABS welds

achieved for dissimilar materials are 83, 80, 65 and 75%, respectively, for welds of ABS to PC, PBT, PEI and M-PPO. Because ABS/ABS welds have a maximum strength that is only about 90.3% of the strength of ABS, another meaningful normalization of weld strengths is to use the strengths of ABS/ABS welds as a baseline. The maximum relative weld strengths of ABS/PC, ABS/PBT, ABS/PEI and ABS/M-PPO achieved are then 92, 89, 72 and 84%, respectively. In contrast to these results, welds of PC/PBT and PC/PEI can attain the strengths of the weaker of the two materials.

Some final comments should be made regarding the effects of penetration and weld pressure on weld strength. Although the weld strengths of most of the dissimilar materials examined tended to rise at higher penetrations and fall at higher weld pressures, this was not always the case. In part, these variations reflect the fact that the basic microstructural and molecular factors affecting weld strength (e.g. flaws, intermolecular diffusion, mechanical interlocking etc.) are not uniquely related to weld pressure and penetration. Moreover, they are often strongly affected by the temperature gradients that develop during the course of welding. These gradients were not characterized in this study. With the availability of such data and a more complete morphological characterization of all of the welded pairs, a more rigorous parametric analysis will be possible.

ACKNOWLEDGEMENTS

Support provided by GE Plastics is gratefully acknowledged. The contributions of K. R. Conway, who carried out all the tests, are greatly appreciated. Special thanks are due to Julia A. Kinloch for her help and patience during the preparation of this paper.

REFERENCES

1 Stokes, V. K. *Polym. Eng. Sci.* 1988, **28**, 718
2 Stokes, V. K. *Polym. Eng. Sci.* 1988, **28**, 728
3 Stokes, V. K. *Polym. Eng. Sci.* 1988, **28**, 989
4 Stokes, V. K. *Polym. Eng. Sci.* 1988, **28**, 998
5 Stokes, V. K. *Polym. Eng. Sci.* 1989, **29**, 1683
6 Stokes, V. K. and Hobbs, S. Y. *Polym. Eng. Sci.* 1989, **29**, 1667
7 Hobbs, S. Y. and Stokes, V. K. *Polym. Eng. Sci.* 1991, **31**, 502
8 Stokes, V. K. *Polym. Eng. Sci.* 1991, **31**, 511
9 Stokes, V. K. *J. Mater. Sci.* 1992, **27**, 5073
10 Stokes, V. K. *Polymer* 1992, **33**, 1237
11 Gabler, K. and Potente, H. *J. Adhesion* 1980, **11**, 145
12 Potente, H. and Gabler, K. *Plastverarbeiter* 1980, **31**, 203
13 El Barbari, N., Michel, J. and Menges, G. *Kunststoffe* 1986, **76**, 20
14 El Barbari, N., Michel, J. and Menges, G. *Kunststoffberater* 1986, **31**, 63
15 Muschik, H., Radax, M., Dragaun, H. and Eichinger, F. *Kunststoffe* 1986, **76**, 23
16 Michel, P. *Polym. Eng. Sci.* 1989, **29**, 1376
17 Schlarb, A. K. and Ehrenstein, G. W. *Polym. Eng. Sci.* 1989, **29**, 1677
18 Stokes, V. K. *Polym. Eng. Sci.* 1992, **32**, 593
19 Underwood, E. E. 'Quantitative Stereology', Addison-Wesley, Philippines, 1970, p. 27
20 Keitz, J. D., Barlow, J. W. and Paul, D. R. *J. Appl. Polym. Sci.* 1984, **29**, 3131